Applied Physics Express

LETTER

A thin multi-order Helmholtz metamaterial with perfect broadband acoustic absorption

Applied Physics Express 12, 084002 (2019)
https://doi.org/10.7567/1882-0786/ab2f94

LETTER

A thin multi-order Helmholtz metamaterial with perfect broadband acoustic absorption

Chong Rui Liu, Jiu Hui Wu*, Fuyin Ma, Xu Chen, and Zhengrui Yang

School of Mechanical Engineering & State Key Laboratory for Strength and Vibration of Mechanical Structures, Xi'an Jiaotong University, Xi'an 710049, People's Republic of China

*E-mail: ejhwu@mail.xjtu.edu.cn

Received May 5, 2019; revised June 23, 2019; accepted July 5, 2019; published online July 17, 2019

We propose a multi-order Helmholtz metamaterial with deep-subwavelength thickness in which perfect continuous acoustic absorption is achieved within 400 Hz ~ 2800 Hz. The metamaterial is composed of multiple detuned cells, each of which is constructed by several perforated plates inserting into the cavity of a Helmholtz resonator (HR) and hence gains multiple individually-tuned high-order peaks besides the original HR peak. By precisely designing each peak of the cells, the extra-broadband perfect absorption can be obtained. This kind of metamaterials could possess broad applications in noise control engineering owing to the extraordinary absorption performance and high flexural stiffness.

Supplementary material for this article is available online

Low-frequency sound absorption has been a challenging topic due to the weak energy dissipation in traditional materials, such as microperforated panels (MPP)[1–3] and porous materials.[4–6] In the last two decades, acoustic metamaterials have opened a new perspective for the researchers. A series of metamaterials with subwavelength thickness has been designed to achieve near total low-frequency sound absorption, such as membrane-type metamaterials,[7–11] coiled-up metamaterials[12–16] and coupled subwavelength resonant system.[17,18] Owing to the resonant nature, most of these metamaterials can only obtain a narrow-band performance, which has limited engineering applications.

Until now, only a few works have presented broadband absorption by introducing multiple detuned cells.[19–33] Some kinds of membrane-type materials[19–22] have been reported for low-frequency broadband absorption on the basis of Mei's work.[9] By using the coiled-up method, Liu et al. proposed an absorber based on 6 coiled Fabry–Perot (FP) channels which could achieve perfect absorption within 100 Hz ~ 200 Hz.[23] Chen et al. reported a structure in which two axially channels in series were coiled-up into a layer perpendicular to incident waves for reducing the sample thickness.[24] Another alternative is to use multiple Helmholtz resonators (HR) with coiled-up cavities.[25,26] In Ang et al's work,[27,28] two enclosed parallel cavities in a new plate-type metamaterial were connected by a small hole, and the consequent couplings could provide a new transmission loss peak, which was also enlightening for the sound absorption. But it is worth noting that only the first-order peak of single cell was utilized for the broadband absorption in most current researches. In fact, the bandwidth can be sufficiently further broadened by introducing high-order peaks. In latest research, a sound-absorbing structure including high-order peaks, composed of 16 coiled-up FP channels, was presented by Yang et al.[29] with a thickness of 10.36 cm, in which near-perfect flat absorption was obtained in the range of 400 Hz ~ 3000 Hz. The structure, however, was a little thick since each channel length should still be up to a quarter wavelength of operating frequency; meanwhile, all the peaks of each channel were simultaneously affected by the structure parameters and could not be adjusted separately.

In this work, we propose a new kind of 8 cm thick multi-order Helmholtz metamaterial with a perfect absorption band within 400 Hz ~ 2800 Hz, and the basic unit is comprised of multiple coiled cells, namely multi-order Helmholtz resonators (MHRs), each of which can provide multiple high-order peaks. Compared with those of FP channels, the MHR peaks have lower frequencies and similar bandwidth under the same structural dimensions. The metamaterial hence has a thinner thickness reduced by 22.8% than Yang et al's structure.[29] In particular, each peak can be tuned individually within a certain frequency range, which is very beneficial to critically couple the peaks for the continuous broadband absorption.

The unit of the proposed metamaterial is composed of n detuned MHR cells which are of N different types, as shown in Fig. 1(a). The unit has an incident area $S_0 = L \times W$ and a thickness of H, where L and W represent unit length and width, respectively. The cell has a square cross-section area S_c and a total cavity length of $l_0 = \sum l_i$, where l_i is the length of each layer. The ratio of the cell area to unit area is defined as $\eta = S_c/S_0$. All the cells are coiled up to acquire excellent low-frequency absorption performance with a deep-subwavelength thickness. As illustrated in Fig. 1(c), the MHR cell was constructed by one or more separating plates with a small hole inserting into the interior of a HR, and could exhibit multiple perfect absorption peaks without changing the structural dimensions. It is worth noting that the first peak of the MHR cell can nearly stay the same position as the original HR peak, retaining the original low-frequency absorption performance. By carefully designing the couplings between the cells, the metamaterial with excellent absorption performance is finally obtained with the parameters as: cell number $n = 30$, cell types $N = 14$, length $L = 49$ mm, width $W = 25$ mm and height $H = 80$ mm. In the unit, the orange cells (1, 2) are of 4 orders, green cells (3, 5, 7, 8, 9, 12 and 13) of 2 orders and yellow ones (4, 6, 10, 11 and 14) of 1 order, i.e. common HR. The absorption coefficient of the metamaterial is presented in Fig. 1(d) and compared with that of MPP (one of typical traditional materials) with the same thickness (8 cm). It can be observed that the metamaterial has a better absorption performance than the MPP within the range below 3000 Hz. A perfect continuous absorption spectrum is obtained by the metamaterial in the frequency range of 400 Hz ~ 2800 Hz, while the

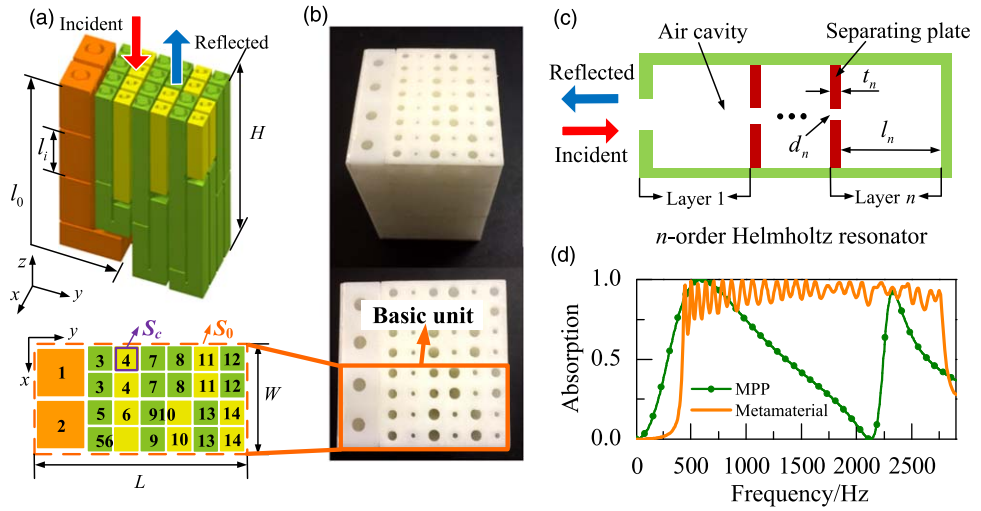

Fig. 1. (Color online) (a) Basic unit of the metamaterial composed of n coiled MHR cells. (b) Photograph of the sample. (c) Cross section of the MHR cell. Green part represents the common HR and the red part is the separating plates. (d) Comparison of the absorption spectrums between the metamaterial and the MPP. The MPP is composed of a 0.2 mm thick aluminum plate perforated by 0.2 mm diameter circular holes with a perforation ratio of 1%. The aluminum plate is backed by an 8 cm cavity.

MPP loses the absorption ability in the middle range of 1200 Hz ~ 2200 Hz resulting in a discontinuous absorption band.

The multi-peak mechanism of the MHR cell is demonstrated by the sound absorption coefficients of cells with different orders, as shown in Fig. 2(a), and the results of the theoretical calculations and finite element simulation show a good agreement (see the supplementary data for the methods of the theoretical calculation and finite element simulation, available online at stacks.iop.org/APEX/12/084002/mmedia). It can be observed that, while the 1-order MHR (common HR) just gains one absorption peak, the 2-order, 3-order and 4-order MHR cells can respectively obtain 2, 3 and 4 near-perfect peaks without changing the external dimensions. In particular, the first peaks of the MHRs ($f = 420$ Hz, 415 Hz and 405 Hz) are all nearly kept in the same frequency as the peak ($f = 415$ Hz) of the 1-order MHR. The inherent generating mechanism is that the original single-degree-of-freedom system is transformed into a multi-degree-of- freedom system by the separating plates with small holes. The acoustic reactance X_s of the MHR can therefore have multiple zero points and the system obtains multiple peak frequencies. On this basis, the corresponding acoustic resistances R_s at each frequency can be close to the characteristic impedance of air medium by the adjustments of the separating plates' parameters, and hence each peak can nearly achieve 100% absorption. As presented in Figs. 2(b) and 2(c), taking 4-order MHR as an example, the relative specific reactance x_s crosses zero at each absorption peak (arrows). The relative specific resistances r_s are 0.90, 1.11, 0.98, and 0.89, respectively, which nearly meets the impedance matching condition. Thus, the absorption coefficients can reach almost 100%. In addition, owing to the large values of the resistances r_s, the 4-order MHR fails to get absorption peaks at other zero points ($f = 780$ Hz, 1570 Hz and 2125 Hz).

The absorption performances of the MHRs and the FP channels with the same external dimensions are compared in Fig. 3(a). The area ratios are both set $\eta = 1/16$. The hole diameters are 2.8 mm and 1.4 mm when $l_0 = 100$ mm, and

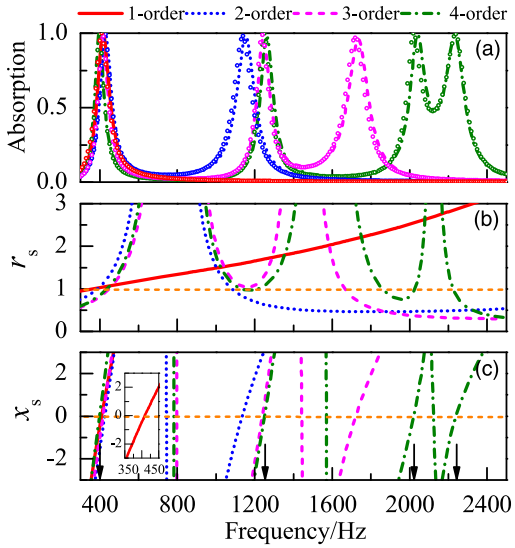

Fig. 2. (Color online) (a) Sound absorption coefficients of the MHRs with different orders (The MHR cavity has a square cross-section area of $S_c = 10$ mm × 10 mm and a total depth of $l_0 = 100$ mm that is equally divided by the separating plates. The area ratio is set $\eta = 1/8$.). The lines correspond to the numerical simulation, while the circles correspond to theoretical calculations. The relative specific resistance r_s (b) and reactance x_s (c) of the MHRs.

2.8 mm, 1.1 mm and 1.3 mm when $l_0 = 150$ mm, respectively. It can be observed that both the MHR and FP channel obtain two near-perfect peaks as the depth is $l_0 = 100$ mm, in particular, the MHR peak frequencies are about 100 Hz and 500 Hz lower than those of the FP channel, respectively. As for $l_0 = 150$ mm, the MHR also gains there absorption peaks with lower frequencies. It can also be found that the peaks of the MHR and FP channel nearly have the same bandwidths. For example, the first peak bandwidths of the MHR and the channel are 42 Hz and 45 Hz, respectively. In addition, one of MHR peak frequencies can be individually tuned in a certain range by adjusting structure parameters with other peak frequencies nearly remaining constant. Figure 3(b) presents the effects of the cavity depths on the absorption performances of a 2-order MHR cell. The area ratio is also $\eta = 1/16$. The

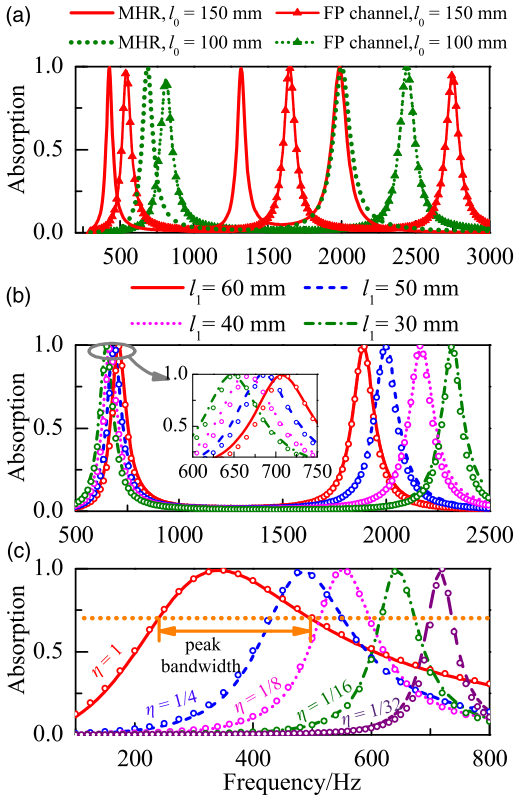

Fig. 3. (Color online) Sound absorption coefficients of (a) the MHRs and the FP channels with different total depths l_0, (b) the 2-order MHR cell with different cavity depths l_1, and (c) the 1-order MHR cell with different area ratio η. The bandwidth refers to the frequency band whose absorption coefficient is above 0.7. The lines correspond to the numerical simulation, while the circles correspond to theoretical calculations.

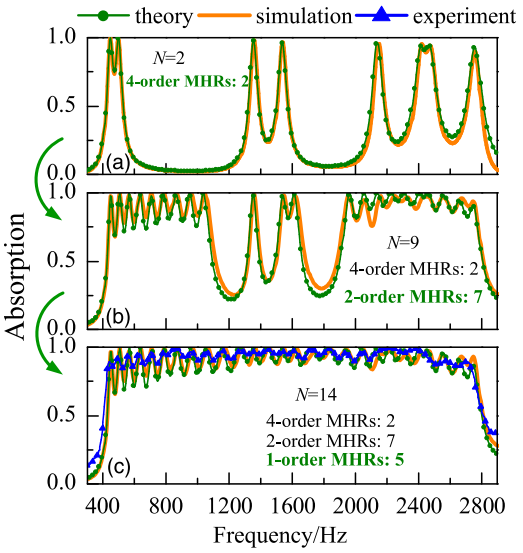

Fig. 4. (Color online) Process to critically couple the cells of the metamaterial with broadband absorption. (a) Absorption using MHR types $N = 2$, (b) absorption using MHR types $N = 9$ and (c) absorption using MHR types $N = 14$.

total depth of the cavity is $l_0 = 100$ mm, and the hole diameters are 2.8 mm and 1.4 mm, respectively. It can be seen that the two peak frequencies are changed with the depth variations, but the peaks can always achieve perfect absorption. While the first peak is slightly shifted to higher frequencies with the increasing depth, the second peak moves to lower frequencies significantly. To a certain degree, it can be claimed that the second peak frequency can be individually adjusted by the depth while the first peak frequency is kept nearly constant. This independent property can help us to obtain peaks in the target positions more easily because the effects of the couplings between the two peaks are weakened, which is a great advantage over the FP channels. It can be therefore concluded that the MHR is a better choice for the sound absorption owing to its lower peak frequencies and independent peaks under the equal bandwidth.

The most effective way to broaden the absorption bandwidth is to introduce multiple detuned cells, but different cell numbers n can bring about the variations of the area ratio η, which can affect the absorption performance of the MHR cell. The specific analysis is conducted by means of a simplified model in which a 1-order MHR cell is adopted with different area ratios η. The total cavity depth is also $l_0 = 100$ mm, and the hole diameters are 0.5 mm, 0.8 mm, 1 mm, 1.4 mm and 2 mm, respectively. Figure 3(c) shows MHR absorption performances, and the results from the simulations and the theoretical calculations agree well. It can be found that, as the area ratio η is decreased, the peak bandwidth ΔB is decreased from 260 Hz to 40 Hz. It is therefore known that the total bandwidth B of a multi-cell structure, which is obtained as $B = n \cdot \Delta B$ with $n = 1/\eta$, can be broadened by the decreased η, but the growth rate is not significant. It increases only from 690 Hz to 1280 Hz when η decreases from 1/8 to 1/32. A balance hence should be reached between the cell number n and the accompanying design and manufacturing difficulties, rather than increasing the number blindly. On the other hand, it is also found that the single peak is shifted from 320 Hz to 710 Hz with the decrease of the ratio η, which is not beneficial to the low-frequency absorption. Therefore, the effects of the area ratio η (or cell number n) on the peak positions should be also considered besides that on the bandwidth. (See supplementary data for detailed explanations.)

For continuous broadband absorption, the metamaterial unit is obtained by critically coupling multiple cells to ensure that all the peaks are distributed uniformly and compactly. Figure 4 depicts the process in detail. The high-order (4-order) MHR cells are firstly designed of which the first peak and the last peak are placed at the lower and upper limits of the absorption band, respectively. Then, $N = 7$ lower-order (2-order) MHRs are utilized to fill the absorption valley, as shown in Fig. 4(b). Most of the valley is raised up by the peaks of 2-order MHRs, but these MHR peaks have a narrow bandwidth owing to the resonant nature. To gain a broader band, the peaks cannot be too close with each other and therefore small dips between them still exists. At last, 1-order MHRs are adopted for the rest of the band valley. The final structure is shown in Fig. 1(a), of which the absorption coefficients are illustrated in Fig. 4(c). The valley disappears and an extraordinary absorption spectrum with small dips is obtained in the low-frequency range of 400 Hz $\sim$ 2800 Hz with the mean absorption coefficient above 95%, which comprises 27 near-perfect absorption peaks. Compared with HR-based structures, this metamaterial obtains 13 more peaks and the bandwidth is dramatically broadened about 100%. What we want emphasize is that this superior absorption performance is not easily achievable since mutual couplings

between the cells due to the surface evanescent waves can also have some effects on absorption performances.[29)]

To verify this result, the metamaterial is fabricated by the 3D printing technology with the acrylonitrile butadiene styrene (ABS) plastic, and measured in a square acoustic impedance tube. The test sample and the measured sound absorption coefficient are shown in Figs. 2(b) and 4(c), respectively. The sample is comprised of two basic units and has a length of 49 mm, a width of 49 mm and a thickness of 80 mm, respectively. Cell 1 has a total cavity depth of $l_0 = 100$ mm which is divided equally by the separating plates. The hole diameters are 4 mm, 2 mm, 2 mm and 2.5 mm, respectively. The impedance tube has a side length of 50 mm, in which only the plane wave can propagate below 3200 Hz. The sample was installed at the end of the tube and measured with the standard two-microphone transfer function method.[34)] Two 1/4 inch condenser microphones were used to record the sound pressure, and a B&K data acquisition system was employed to acquire the sound pressure. It can be found from Fig. 4(c) that the experimental result is basically consistent with the theoretical and numerical results. The slight discrepancy is mainly caused by imperfections in the sample manufacturing. In order to confirm this fact, the correctness of the theoretical approach and finite element simulation model were firstly ensured through the comparisons with relevant studies. The reliability and accuracy of the test system were then verified through a simple structure measured for five times, and the experimental results agreed well with those of the theoretical and numerical methods. Thus, it comes to the conclusion that the discrepancy is mainly resulting from the manufacturing errors of this complicated structure.

In this study, an acoustic metamaterial is proposed with a near-perfect continuous absorption spectrum within 400 Hz ~ 2800 Hz, of which the thickness (8 cm) is reduced to the deep-subwavelength regime. This metamaterial is comprised of multiple detuned MHR cells, each of which can gain multiple absorption peaks by inserting separating plates into the HR cavity. Particularly, the first peak of the MHR cell is kept nearly unchanged with the original HR peak. Compared with the HR-based structures, the bandwidth can be dramatically broadened about 100% in the low-frequency range by the MHR cells. Besides, the MHR cells can acquire peaks with lower frequencies and similar bandwidth than the FP channels. The proposed metamaterial would offer a new approach to the investigations of the broadband absorption and has great future applications in the noise reductions of rooms, plants, automotive industry and aerospace engineering. See the supplementary data for the methods of the theoretical calculation and finite element simulation, and the detailed explanations for the effects of the area ratios on the absorption performances.

Acknowledgments This work was supported by the National Natural Science Foundation of China (NSFC) under Grant No. 51675401 and 51705395.

ORCID iDs Chong Rui Liu https://orcid.org/0000-0003-2631-9717 Fuyin Ma https://orcid.org/0000-0003-0493-6132

1) D. Y. Maa, J. Acoust. Soc. Am. **104**, 2861 (1998).
2) H. V. Fuchs and X. Zha, Acta. Acust. United **92**, 139 (2006).
3) J. Liu and D. W. Herrin, Appl. Acoust. **71**, 120 (2010).
4) H. Meng, Q. B. Ao, S. W. Ren, F. X. Xin, H. P. Tang, and T. J. Lu, Compos. Sci. Technol. **107**, 10 (2015).
5) T. Dupont, P. Leclaire, O. Sicot, X. L. Gong, and R. Panneton, J. Appl. Phys. **110**, 094903 (2011).
6) W. H. Chen, F. C. Lee, and D. M. Chiang, J. Sound Vib. **237**, 337 (2000).
7) Z. Yang, J. Mei, M. Yang, N. H. Chan, and P. Sheng, Phys. Rev. Lett. **101**, 204301 (2008).
8) S. H. Lee, C. M. Park, Y. M. Seo, Z. G. Wang, and C. K. Kim, Phys. Rev. Lett. **104**, 054301 (2010).
9) J. Mei, G. Ma, M. Yang, Z. Yang, W. Wen, and P. Sheng, Nat. Commun. **3**, 756 (2012).
10) K. Lu, J. H. Wu, D. Guan, N. Gao, and J. Li, AIP Adv. **6**, 025116 (2016).
11) M. Yang, C. Meng, C. Fu, Y. Li, Z. Yang, and P. Sheng, Appl. Phys. Lett. **107**, 104104 (2015).
12) Y. Li and B. M. Assouar, Appl. Phys. Lett. **108**, 063502 (2016).
13) X. Cai, Q. Guo, G. Hu, and J. Yang, Appl. Phys. Lett. **105**, 121901 (2014).
14) Z. Liang and J. Li, Phys. Rev. Lett. **108**, 114301 (2012).
15) Y. Li, B. Liang, X. Tao, X. F. Zhu, X. Y. Zou, and J. C. Cheng, Appl. Phys. Lett. **101**, 233508 (2012).
16) Y. Xie, B. I. Popa, L. Zigoneanu, and S. A. Cummer, Phys. Rev. Lett. **110**, 175501 (2013).
17) H. Long, Y. Cheng, J. Tao, and X. Liu, Appl. Phys. Lett. **110**, 023502 (2017).
18) J. Li, W. Wang, Y. Xie, B. I. Popa, and S. A. Cummer, Appl. Phys. Lett. **109**, 091908 (2016).
19) G. Ma, M. Yang, S. Xiao, Z. Yang, and P. Sheng, Nat. Mater. **13**, 873 (2014).
20) C. R. Liu, J. H. Wu, K. Lu, Z. T. Zhao, and Z. Huang, Appl. Acoust. **148**, 1 (2019).
21) F. Ma, M. Huang, and J. H. Wu, J. Appl. Phys. **122**, 215102 (2017).
22) F. Ma, M. Huang, Y. Xu, and J. H. Wu, Sci. Rep. **8**, 5906 (2018).
23) C. Zhang and X. Hu, Phys. Rev. Appl. **6**, 064025 (2016).
24) C. Chen, Z. Du, G. Hu, and J. Yang, Appl. Phys. Lett. **110**, 221903 (2017).
25) Y. Wang, H. Zhao, H. Yang, J. Zhong, D. Zhao, Z. Lu, and J. Wen, J. Appl. Phys. **123**, 185109 (2018).
26) F. Ma, J. Chen, and J. H. Wu, J. Mater. Chem. C **7**, 5131 (2019).
27) L. Y. L. Ang, Y. K. Koh, and H. P. Lee, Appl. Phys. Lett. **112**, 051903 (2018).
28) L. Y. L. Ang, Y. K. Koh, and H. P. Lee, Appl. Acoust. **140**, 160 (2018).
29) M. Yang, S. Chen, C. Fu, and P. Sheng, Mater. Horiz. **4**, 673 (2017).
30) Z. Jia, J. Li, C. Shen, Y. Xie, and S. A. Cummer, J. Appl. Phys. **123**, 025101 (2018).
31) C. R. Liu, J. H. Wu, X. Chen, and F. Ma, J. Phys. D: Appl. Phys. **52**, 105302 (2019).
32) N. Gao, Z. Wei, H. Hou, and A. O. Krushynska, J. Acoust. Soc. Am. **145**, EL79-EL83 (2019).
33) N. Jiménez, V. Romero-García, V. Pagneux, and J. P. Groby, Sci. Rep. **7**, 13595 (2017).
34) ISO 10534-2:1998, ISO Standard: Acoustics–Determination of sound absorption coefficient and impedance in impedance tubes–Part 2: Transfer function method (International Organisation for Standardisation, Geneva, 1998).
35) J. Kergomard and A. Garcia, J. Sound Vib. **143**, 465 (1987).
36) V. Dubos, J. Kergomard, A. Khettabi, J. P. Dalmont, D. H. Keefe, and C. J. Nederveen, Acta Acust United Acust **85**, 153 (1999).
37) M. R. Stinson, J. Acoust. Soc. Am. **89**, 550 (1991).
38) T. Liu, S. Liang, F. Chen, and J. Zhu, J. Appl. Phys. **123**, 091702 (2018).